International Journal of Heat and Mass Transfer 54 (2011) 4913–4922

Contents lists available at ScienceDirect

International Journal of Heat and Mass Transfer

journal homepage: www.elsevier.com/locate/ijhmt

Evaporation characteristics of fuel droplets with the addition of nanoparticles under natural and forced convections

Yanan Gan, Li Qiao *

School of Aeronautics and Astronautics, Purdue University, West Lafayette, IN 47907, USA

ARTICLE INFO

Article history:
Received 1 May 2011
Received in revised form 28 June 2011
Accepted 28 June 2011
Available online 23 July 2011

Keywords:
Nanofluids
Nanoparticle
Fuel droplet
Evaporation rate
D^2-law
Particle aggregation

ABSTRACT

Evaporation characteristics of fuel droplets containing suspended aluminum nanoparticles were determined under natural and weak forced convections at varying flow temperatures. The results show that under higher convection temperatures droplet evaporation follows the classical D^2-law. Under low forced convection temperatures or natural convection, however, a departure from the classical D^2-law was observed and the evaporation rate gradually slowed. A modeling based on the population balance equation was performed to understand the dynamic particle aggregation process. The modeling results suggest that particle aggregation is likely the cause of the D^2-law-deviation phenomena.

1. Introduction

Nanofluids, an exciting new class of nanotechnology-based heat transfer fluids, have received much interest in recent years [1–3]. They are liquids with the stable suspension of a small amount of nanometer-sized particles (e.g., metals, oxides, carbides, nitrides, or carbon nanotubes) having typical lengths of 1–100 nm. Nanofluids have been discovered to have significantly enhanced thermal conductivity and can be used for a variety of energy/thermal systems, such as electronic cooling and microelectromechanical systems (MEMS). Besides heating and cooling purposes, nanofluids can also be applied in other areas. Senthilraja et al. [4] provided a comprehensive review of the applications of nanofluids in automobiles as a coolant, fuel additive, lubricant, shock absorber, and refrigerant.

The present study is based on a new concept in the field of combustion and fuels: tailored nanofluid-type fuels created by properly mixing nanoscale materials such as energetic metals with traditional liquid fuels. Energetic nanomaterials offer high reactivity, fast ignition, and fast energy release [5]. When mixed with liquid fuels, they can increase the volumetric energy density of the fuel, which is the most important parameter of fuel for high-speed propulsion systems. The nanofluid-type fuels comprise a new class of fuels and have been rarely studied. Jackson et al. [6] measured the ignition delay time of slurries of n-dodecane and nano-aluminum particles in a shock tube, demonstrating that the addition of nano-aluminum could substantially decrease the ignition delay time. Using a simple hot-plate experiment, Tyagi et al. [7] found that the ignition probability for fuel mixtures that contained aluminum nanoparticles was significantly higher than that of pure diesel. Gan and Qiao [8] recently compared the burning characteristics of fuel droplets with nano- and micron-sized aluminum particles. The results reveal that for the same solid loading rate and surfactant concentration, the disruption and microexplosion behavior of the micron suspension occurred later with much stronger intensity. Moreover, the authors show that particle collision and aggregation behavior play an important role in the overall burning characteristics of fuel droplets.

In practical combustion systems such as diesel engines, gas turbines, and rocket engines, as well as oil-fired boilers, liquid fuel is sprayed into the combustion chamber as a cloud of droplets [9]. When the droplets are exposed to a hot environment, they evaporate quickly. In fact, droplet evaporation is an important process in the combustion of liquid fuels and is also important for nanofluids with applications in boiling heat transfer. However, studies on the evaporation behavior of nanofluids are rare. Chon et al. [10] investigated the evaporation and dry-out characteristics of a strongly pinned water droplet with nanoparticles on a heated substrate and identified three periods: liquid dominant evaporation, dry-out progress, and nanoparticle strain. Sefiane and Bennacer [11] studied evaporation kinetics and wetting dynamics of ethanol-based sessile nanofluid droplets on rough heated substrates. A reduction of evaporation rate compared to the base fuel was found during the pinning phase. Considering three different types of

* Corresponding author. Address: 701 W. Stadium Ave., West Lafayette, IN 47907-2045, USA. Tel.: +1 765 494 2040; fax: +1 765 494 0307.
E-mail address: lqiao@purdue.edu (L. Qiao).

0017-9310/$ - see front matter © 2011 Elsevier Ltd. All rights reserved.
doi:10.1016/j.ijheatmasstransfer.2011.07.003

Nomenclature

D	droplet diameter (m)
k	Boltzmann constant (1.38×10^{-23} m^2 kg s^{-2} K^{-1})
K	droplet evaporation rate (mm^2/s)
n_i	number of the i-fold aggregate
r_i	radius of the i-fold aggregate (m)
S_i	breakup rate of the i-fold aggregate (s^{-1})
t	time (s)
T	temperature (K)

Greek symbols

α_{ij}	collision efficiency
β_{ij}	collision frequency (m^3/s)
Γ_i	distribution function
μ	viscosity (kg m^{-1} s^{-1})

Subscripts

i	i-fold aggregate
j	j-fold aggregate

nanoparticles, Chen et al. [12] studied the effects of nanoparticles on the evaporation process of deionized water. They observed a unique behavior; that is, the evaporation rate changed from one constant to another after reaching a critical time, which they call transition phenomena. This phenomenon was explained based on the nanofluid's apparent heat of vaporization.

Previous studies on the evaporation of nanofluids have provided important insights, but many questions remain. For example, the mechanism responsible for the transition behavior Chen et al. [12] observed has not been well understood. Furthermore, the effects of particle aggregation on droplet evaporation rate have not been carefully considered. We have shown in a previous study that particle aggregation has a significant impact on droplet combustion behavior [8]. Motivated by this, we investigated the evaporation characteristics of fuel droplets with the addition of energetic nanoparticles under various conditions.

The objectives of the paper are first to experimentally determine the evaporation rate by considering various base fuels with addition of nanoparticles at varying concentrations under natural and forced convections; second, to model the dynamic particle aggregation process inside a vaporizing droplet and to determine its effect on the evaporation rate. The paper starts with a brief description of fuel preparation and characterization methods, after which the experimental method is introduced. We then discuss the evaporation characteristics of different types of fuel droplets, e.g., the effects of base fuel, particle concentration, and flow temperature. In particular, the deviation from the D^2-law phenomenon is reported and discussed. Lastly, we discuss a model that we built based on the population balance equation (PBE), which we solved to simulate particle aggregation dynamics inside an evaporating droplet. The simulation results help to explain the D^2-law deviation phenomenon observed in the experiment.

2. Experimental methods

2.1. Fuel preparation and characterization

Two liquid fuels, n-decane and ethanol, were considered as the base fuel. Their physical properties are shown in Table 1. Aluminum nanoparticles purchased from Nanostructured & Amorphous Materials, Inc. have a mean diameter of 80 nm. Fig. 1 shows an SEM photograph of the nano-Al samples. Most particles are spherical, and the size distribution is in the range of 35–100 nm.

The method used to disperse particles evenly in base fuel was described in a previous study [8]. Here we will only briefly discuss the preparation process. The challenge was to form a stable, homogenous mixture with a minimum degree of particle agglomeration. Sonication [13] and addition of a surfactant are generally used as a means to reduce particle agglomeration and to promote stabilization of the suspension. At first, particles were mixed with liquid fuels and vigorously stirred by hand. The mixture was then sonicated using an ultrasonicator; this was performed in an ice bath for about 5 min. In some mixtures, a surfactant (Sorbitan Oleate) was added before sonication to promote chemical stabilization of the suspension.

After sonication, suspensions of ethanol/nano-Al (1 wt.%) can last for 24 h without obvious sedimentation. However, n-decane/nano-Al (1 wt.%) typically can remain stable for only 20 min, beyond which sedimentation was observed. To promote suspension stability, Sorbitan Oleate was added to them as a chemical agent. The maximum concentration of added surfactant was 0.5 wt.%, and with this the n-decane/nano-Al suspension can maintain stable for more than 5 h, much longer than suspensions without surfactant. This is because of the steric stabilization mechanism of surfactant [14]. We have explained in a previous study [8] that ethanol-based suspensions can last much longer than n-decane-based suspension because ethanol has a higher viscosity than n-decane and also because of ethanol's ability to form gel structures around the particles [15].

2.2. Experimental setup and data analysis

Fig. 2 shows a schematic of the droplet evaporation experiment. The setup consists of a droplet suspension system, a heated nitrogen flow, a high-speed camera, and a data acquisition system. Droplets with a diameter of about 1 mm were suspended on the welding point of a thin thermocouple (75 μm). To control the size of a suspended droplet, a syringe pump was adjusted to run at a low flow rate, which produced a droplet at a desired size at the tip of the needle. It was then transferred on the thermocouple. A

Table 1
Physical properties of n-decane, ethanol and Sorbitan Oleate.

	Chemical formula	Molecular weight	Boiling point (K at 1 atm)	Viscosity (mPa s at 20 °C)
n-Decane	$C_{10}H_{22}$	142	447	0.92
Ethanol	C_2H_6O	46	352	1.2
Sorbitan Oleate	$C_{24}H_{44}O_6$	428	852	1200–2000

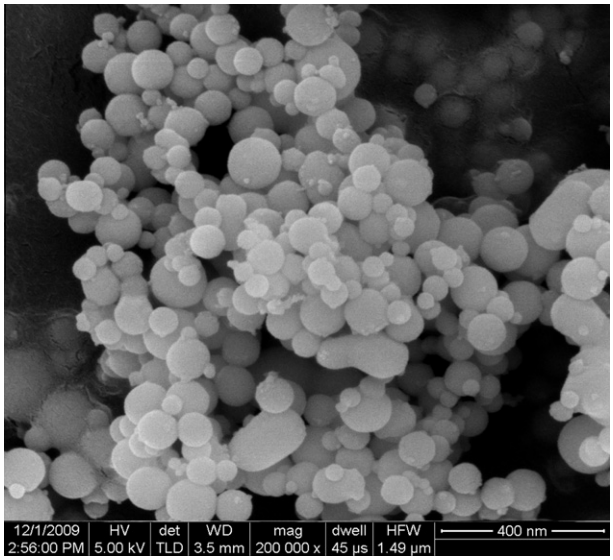

Fig. 1. SEM photograph of aluminum nanoparticles with a mean diameter of 80 nm [8].

glass shield was placed around the droplet to avoid disturbances from the environment and to provide optical access.

Droplets were either vaporized under natural convection at room temperature or under weak forced convection at elevated temperatures of up to 500 K. This was achieved by flowing a preheated nitrogen flow around the droplet. Nitrogen was heated when flowing through a coil made of stainless steel that was wrapped with heating tape. The temperature of the heating system was controlled by a feedback temperature controller. Nitrogen was selected because it can avoid potential oxidation and burning of fuel droplets at higher temperatures. The heated nitrogen flow passed a honeycomb and glass beads, which created a uniform laminar flow around the droplet.

A high-speed digital camera coupled with a microlens was used to record droplet evaporation history. An adjustable extension tube was placed between the camera and the microlens to get a magnified view of the droplet. A light source was on the opposite side of the camera to backlight the droplet. A thin thermocouple was used to suspend the droplet and also to record its temperature. One was also placed below the droplet to monitor the temperature of the nitrogen flow. Both were type-K thermocouples. The temperature data were acquired by a 1000-Hz data acquisition system synchronized with the high-speed camera.

After the droplet was placed on the tip of the thermocouple, the camera and the temperature data acquisition system were simultaneously triggered. For each experiment, about 6000 images and temperature values were recorded to achieve a satisfactory time resolution. The microlens and the camera were placed 10 cm from the droplet, and the magnification was kept constant. The resolution of the high-speed camera was set to be 256 × 256 pixels with 8 bits for each pixel. A grid with known size was placed in the same position as the droplet, and the spatial resolution of imaging was thus determined to be 6–7 μm per pixel.

To postprocess the many images, a Matlab code was developed to determine droplet size history, from which droplet evaporation rate could be derived. A threshold value for pixel gray level was carefully set to count the pixels in the droplet zone. The droplet size was then calculated from the number of pixels. Lastly, at least three tests were carried out for each experimental condition to validate the repeatability of the experiment. The uncertainties of the evaporation rate measurements were estimated within ±3%.

3. Results and discussion

3.1. Typical droplet evaporation process

In this section, we will discuss the general characteristics of the entire droplet evaporation process, e.g., droplet size and temperature histories, and how we used and interpreted the data. After the droplet was positioned on the joining point of the thermocouples, data acquisition systems were triggered, and nitrogen was flowed through the test section.

Fig. 3 shows the typical droplet size and temperature histories for an ethanol-based fuel droplet under weak convection with a nitrogen flow temperature of 335 K. The droplet contains 2.5% (by weight) aluminum nanoparticles with an average size of 80 nm. Three distinct stages were identified based on the synchronized droplet size and temperature curves: natural convection, weak forced convection, and dry-out stage. The ethanol droplet was initially under natural convection before the heated nitrogen

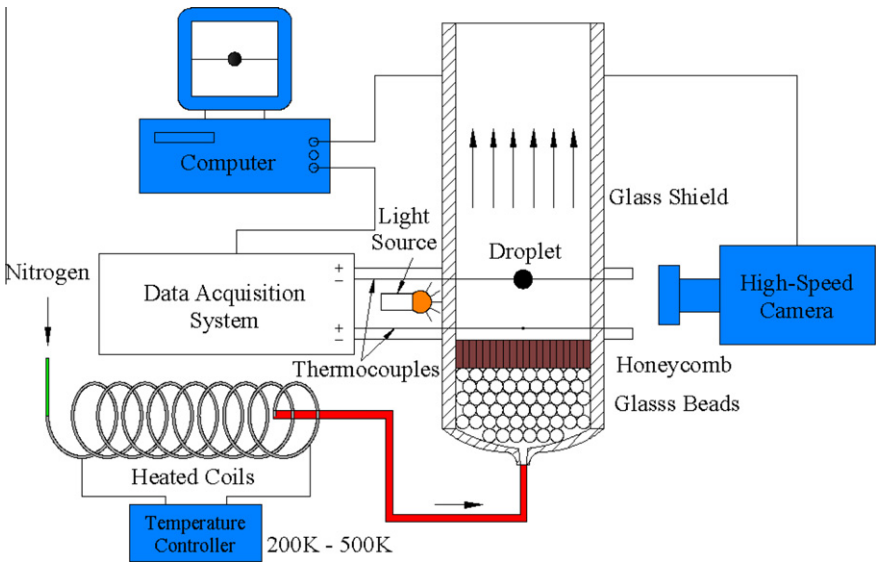

Fig. 2. Schematic of the experimental setup.

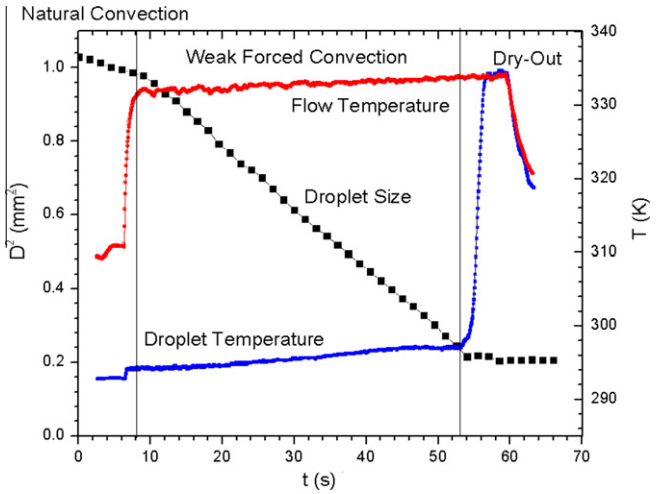

Fig. 3. Typical droplet size and temperature history for ethanol-based fuel (2.5% nano-Al).

stream flowed through it. In this stage, the droplet size decreases slightly as a result of natural evaporation. During the second stage, the heated nitrogen stream was applied, which resulted in a steep rise in the flow temperature. The droplet temperature was also slightly elevated. A steady-state evaporation process was established after a short time (about 3 s), in which the square of the droplet size regresses linearly with respect to time. During the steady-state evaporation stage, the flow temperature remained almost the same, and the droplet temperature gradually increased by 5 K. The overall temperature difference between gas flow and droplet was about 40 K during this stage. In the final stage, all liquid in the droplet had been vaporized, and an agglomerate of about 100 μm was left on the fiber. The flow and droplet temperatures quickly dropped after the nitrogen flow was shut off.

Fig. 4 shows the typical droplet size and temperature histories of an n-decane-based droplet under weak convection with a nitrogen flow temperature of around 335 K. The mass ratio of the added nanoparticles is the same as in the ethanol-based droplet, 2.5%. Similarities are found between Figs. 3 and 4. However, differences exist and are discussed below. First, the temperature difference between droplet and gas flow is about 5 K, lower than the 40 K difference for the ethanol-based droplet. Second, the droplet temperature rises to reach the same temperature of the gas flow before the dry-out stage. The droplet size regresses nonlinearly during the latter stage of the evaporation process. Lastly, the lifetime of the droplet is longer for the n-decane-based droplet than for the ethanol-based droplet (210 s vs. 70 s) because of n-decane's higher boiling point than ethanol's. Having discussed the entire droplet evaporation process, it is important to note that for all experiments only the steady-state evaporation process was considered in the analysis.

3.2. Evaporation of pure liquid droplets

The evaporation rate of pure liquid was measured first as a baseline to understand the effect of various added nanoparticles on droplet evaporation behavior. Fig. 5 shows the evaporation rate of an ethanol droplet under natural convection at 300 K and under weak forced convection at various flow temperatures (300–380 K). It is clear that the droplet size variation with time follows the classical D^2-law under all conditions, which comes from Langmuir's original work [16]. Note that the droplet diameter D was scaled by the original droplet diameter D_0, as suggested by the classical theory of droplet evaporation [9].

3.3. Evaporation of ethanol-based droplets with the addition of nanoparticles

In this section, we will discuss the evaporation characteristics of ethanol droplets containing Al nanoparticles at various concentrations under natural and forced convections. Fig. 6 shows the droplet size as a function of time for ethanol droplets with the addition of 0.5 wt.% nano-Al under various temperatures. Under weak forced convection at temperatures of 330 K and 380 K, the droplet size regresses following the classical D^2-law. The evaporation rate under weak forced convection at room temperature (300 K) also approximately follows the D^2-law. The variation of droplet sizes under natural convection at room temperature (300 K), however, shows a feature that deviates from the D^2-law – the curve is "bent." The instantaneous droplet evaporation rate was plotted here as a function of time in Fig. 7 (dash line). It can be seen that this rate decreases all the way until the very end where it shows a slight bounce back. The minimum evaporation rate occurs around t = 250 s, and a 36% reduction was observed (to 0.0016 mm^2/s, from 0.0025 mm^2/s).

The results for ethanol droplets containing a higher concentration (2.5 wt.%) of nano-Al particles are shown in Fig. 8. It seems

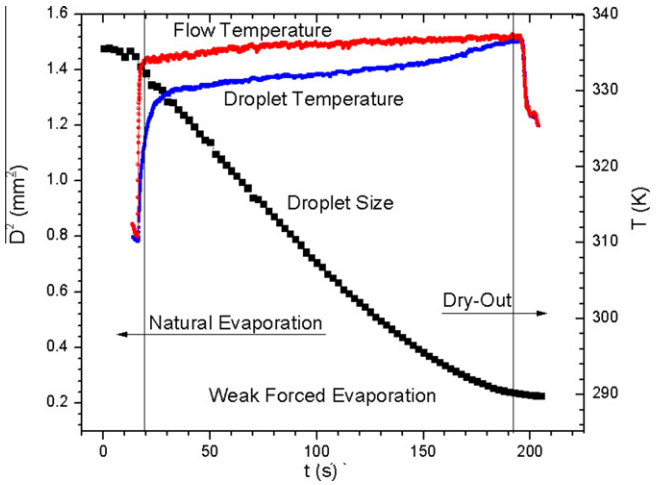

Fig. 4. Typical droplet size and temperature history for n-decane-based fuel (2.5% nano-Al).

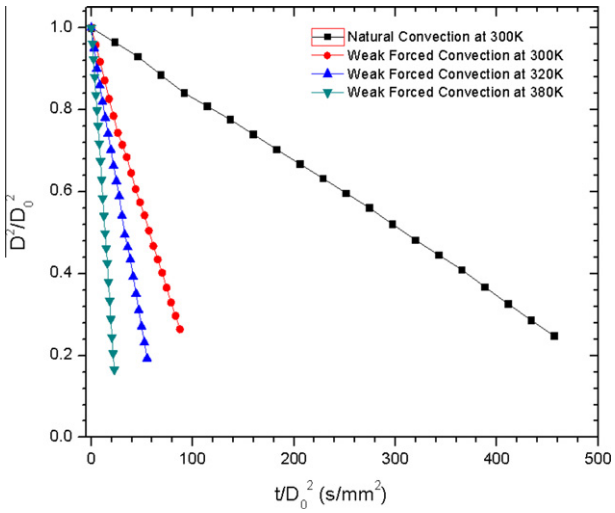

Fig. 5. Evaporation of ethanol droplets under different temperatures.

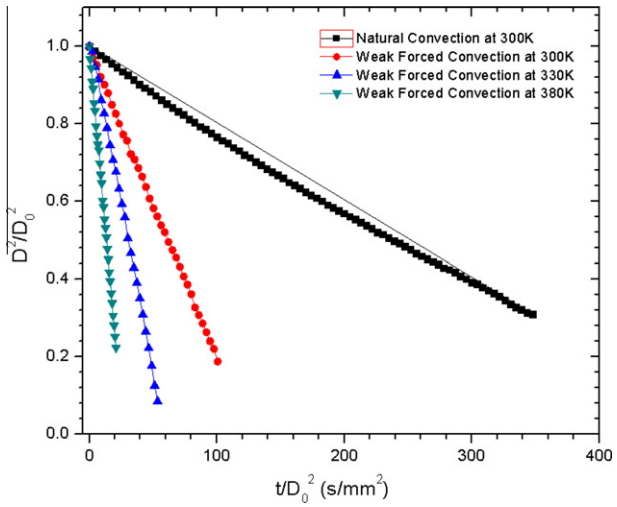

Fig. 6. Evaporation of ethanol droplets with 0.5% nano-Al under different temperatures.

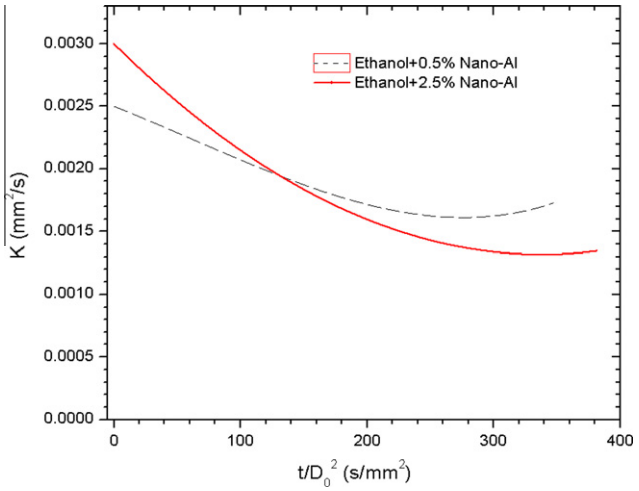

Fig. 7. Evaporation rate of ethanol droplets with nano-Al under natural evaporation at 300 K.

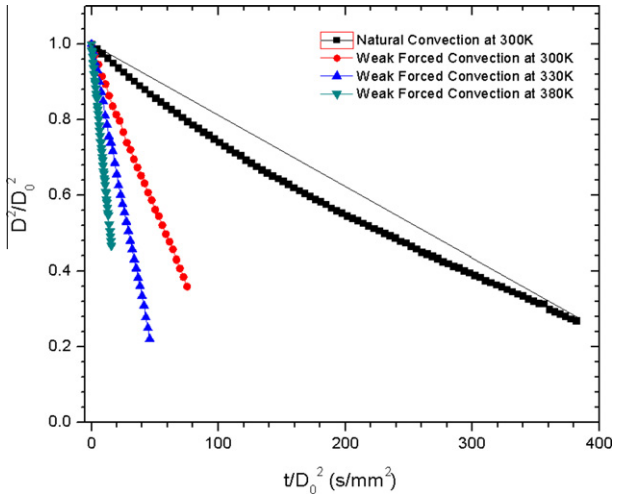

Fig. 8. Evaporation of ethanol droplets with 2.5% nano-Al under different temperatures.

that the droplet-size history follows the D^2-law under weak forced convection of various flow temperatures (300 K, 330 K, and 380 K). Under natural convection at room temperature (300 K), however, the square of the droplet size clearly deviates from the D^2-law. Also, the bending of the curve is more prevalent than for the droplet containing 0.5 wt.% nano-Al particles shown in Fig. 6. In other words, the deviation from the D^2-law is more significant at higher particle concentrations. The instantaneous evaporation rate for the droplet with 2.5 wt.% nano-Al was also plotted as a function of time in Fig. 7 (solid line). The evaporation rate decreases continuously. A reduction of about 50% in the evaporation rate was observed (to below 0.0015 mm^2/s, from 0.0030 mm^2/s), which is higher than the reduction for the droplet with 0.5 wt.% nano-Al.

3.4. Evaporation of n-decane-based droplets with the addition of nanoparticles

In this section, we will discuss the evaporation characteristics of n-decane-based droplets containing nanoparticles. Compared to ethanol, n-decane is a high-boiling-point fuel and requires a longer time for complete evaporation. Fig. 9 shows the droplet size histories of n-decane-based fuel droplets with the addition of 0.5 wt.% nano-Al particles under various conditions. At higher temperatures (320 K and 380 K) under weak forced convection, the droplet size variation obeys the D^2-law. However, the law's deviation phenomenon occurs under weak convection at room temperature (300 K). As a comparison, under the same condition the evaporation of ethanol-based droplets containing either 0.5 wt.% or 2.5 wt.% nano-Al particles still follows the D^2-law. Note that the evaporation process of n-decane-based fuels under natural convection at 300 K is not shown in the figure because the droplet lifetime is much longer (about 2 h) than the others, but the D^2-law deviation phenomenon is quite obvious under this condition.

The results for n-decane-based droplets containing 2.5 wt.% nano-Al particles are shown in Fig. 10. The D^2-law deviation phenomenon occurs at 300 K and 320 K under weak forced convection. Moreover, the curve at 300 K is more "bent" for 2.5 wt.% nano-Al particle addition than from the 0.5 wt.% nano-Al particle addition. This is consistent with the results of the ethanol-based droplets – the deviation from the D^2-law is more significant at higher particle concentrations. Under even higher temperatures (such as 380 K), the droplet size history follows the D^2-law. The droplet lifetime of n-decane-based fuels is found to be much longer than that of ethanol-based fuels (650 s vs. 100 s).

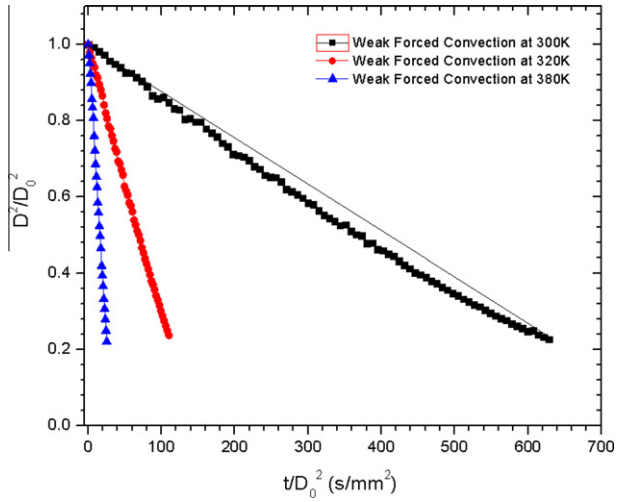

Fig. 9. Evaporation of n-decane droplets with 0.5% nano-Al under different temperatures.

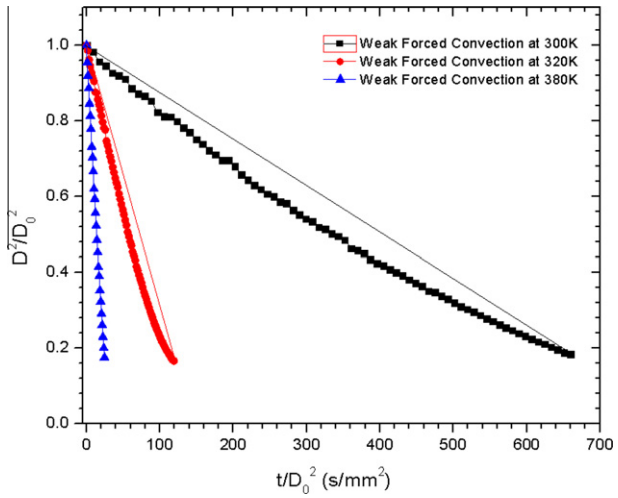

Fig. 10. Evaporation of n-decane droplets with 2.5% nano-Al under different temperatures.

Similarly, the instantaneous droplet evaporation rate for n-decane-based droplets with 0.5 wt.% and 2.5 wt.% nano-Al addition was plotted as a function of time in Fig. 11. For both, the evaporation rate decreases with time. For the n-decane-based droplet with 0.5 wt.% nano-Al, a 48% reduction was observed (to 0.00073 mm^2/s, from 0.0014 mm^2/s). For the n-decane-based droplet with 2.5 wt.% nano-Al, a higher (53%) reduction in evaporation rate was observed (to 0.0008 mm^2/s, from 0.0017 mm^2/s).

3.5. Comparison with previous experiments

In summary, the experimental results show that the deviation from the D^2-law phenomenon is more significant at higher particle concentrations than at lower ones, assuming that the other conditions (such as base fluid and flow convection environment) are the same. The deviation is more obvious at lower convection temperatures than at higher ones for the same base fluid and at the same particle concentration. With regard to various base fluids, the deviation is more obvious for higher boiling point fuels than for lower ones. Although several factors may contribute to the D^2-law deviation behavior, there is a common feature for all the experiments in which deviation was observed – the droplet lifetime is much longer, compared to the droplet lifetime in the experiment for which the D^2-law obeys. The droplet lifetime seems to play a role in whether the evaporation follows or deviates from the D^2-law.

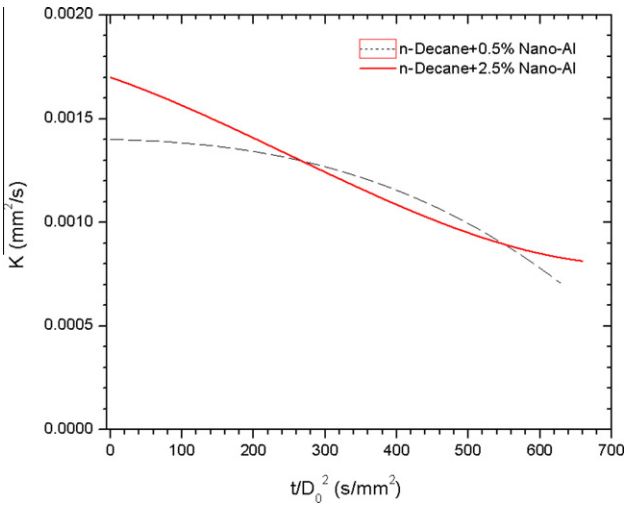

Fig. 11. Evaporation rate of n-decane droplets with nano-Al under weak evaporation at 300 K.

Chen et al. [12] studied the effect of three nanoparticles (laponite, Fe_2O_3, and Ag) on the evaporation rate of deionized water under natural convection at room temperature. The results show that the evaporation may be enhanced or slowed down, depending on the type of nanoparticle and whether it is used in combination with the surfactant PVP. In particular, the evaporation rate of various Ag and Fe_2O_3 nanofluids goes through a transition from one constant value to another during the evaporation process. The authors explained the effect of various nanoparticles on evaporation from the perspective of apparent heat of evaporation. The addition of nanoparticles generally increases the apparent heat of evaporation and thus reduces the evaporation rate. The authors also suggested that the transition phenomenon was caused by the increasing particle concentration during the droplet evaporation process as the droplet volume became smaller.

The present experiment deals with different base fluids (mainly liquid hydrocarbon fuels) and nanoparticles (reactive metal particles) with an interest in burning these nanofluid-type fuels. Further, it considered both natural convection and weak forced convection. Some of our results are consistent with the observations of Chen et al. [12]. For instance, nanofluid droplets vaporize as a pure liquid droplet at the beginning stage, and nanoparticles inside the droplet generally tend to slow down the droplet evaporation rate. However, we did not observe the transition phenomenon, that is, the evaporation rate K changes from one constant value to another constant after a critical time is reached. Instead, our finding was that the evaporation rate K varies throughout the entire evaporation process in situations in which the D^2-law does not apply.

Possibly the addition of particles changes the apparent heat of evaporation and thus modifies the evaporation behavior. Particles could also change the viscosity and surface tension of the fluid, which in turn could impact evaporation. Nevertheless, the effect of particle aggregation behavior on droplet evaporation has not been seriously considered. During the evaporation process of a multicomponent (liquid + solid) droplet, there are two major events: fluid dynamics and particle dynamics. Fluid dynamics means the motions associated with the fluid component, including droplet surface regression, internal circulation, and liquid diffusion from inside to surface. Particle dynamics means the motions associated with particles, e.g., particle collision, particle aggregation, and aggregate breakup. The motions of the two components are indeed coupled. For instance, fluid motion could impact particle aggregation. On the other hand, particle aggregation could also affect fluid dynamics and thus impact evaporation.

Motivated by this, we modeled the particle aggregation process inside a droplet. Our goal here is not to develop or validate aggregation kinetics. In fact, simulating the detailed transient aggregation process is a challenging task. This is because the rate parameters and coefficients that appeared in the PBE are largely unknown, e.g., the collision efficiency between clusters with various sizes and structures, and the breakup coefficient of larger structures to smaller ones. This is mainly responsible for the remarkable differences between theoretical predictions and experimental results. Another factor making the simulations extremely challenging is that primary particles can form aggregates that have various shapes and densities. And it is impossible to predict the detailed structure of the aggregates. To solve this problem, aggregates are usually modeled as fractals using fractal dimension as an additional variable in the population balance equation [17]. Our goal here is to qualitatively understand the aggregation process inside an evaporating droplet and how this process could potentially impact the droplet evaporation rate, especially the D^2-law deviation behavior.

3.6. Modeling of the particle aggregation process

The goal of the modeling work is to understand the transient aggregation process of nanoparticles inside a vaporizing droplet under natural or forced convections. This may help to explain the experimental observations, especially the D^2-law deviation phenomenon. In the present study, the evolution history of particle aggregates (including aggregation size and distribution) were obtained by solving the PBE. This is a classical method of modeling the evolution of particulate systems by accounting for various events taking place between particles in the population, e.g., aggregation and breakage. Kumar and Ramkrishna [18] has provided a comprehensive review of the application of population balance equations in particulate systems. In the following, we will describe formation of the model and the numerical method used to solve the equation sets, and then we will discuss the results and how they can be used to understand the effect of particle aggregation on droplet evaporation rate.

3.6.1. Description of the model and the numerical method

Particle aggregation is a result of collisions between particles. Thus the aggregation process depends on collision frequency and collision efficiency. According to Fendler and Dekany [19], there are three major transport mechanisms responsible for particle aggregation in nanofluids: Brownian diffusion, fluid motion, and differential setting. The Brownian motion means the random movements of small particles. It is also called perikinetic collisions and has been studied widely by the nanoscience community. The second mechanism (fluid motion) means the relative motion of particles induced by fluid transport, e.g., shear flow and agitation. This mechanism is also called orthokinetic aggregation [19], and it can significantly increase the chance of collisions between particles, especially for large particles. The third mechanism is because of gravity – when particles of different sizes and densities are settling in a nanofluid, they tend to capture other particles as they fall.

The model describes the dynamic aggregation process of Al nanoparticles (80 nm) in a vaporizing fuel droplet (ethanol and n-decane), as shown in Fig. 12. To match the experimental conditions, the droplet in the modeling has sphere geometry with a diameter of 1 mm. Initially, Al nanoparticles were uniformly distributed within the droplet. The collision frequency between particles becomes higher as the droplet is being vaporized because particle concentration becomes higher. After a sufficiently long time, it is possible that all particles adhere and form one or a few large agglomerates when all liquid is consumed.

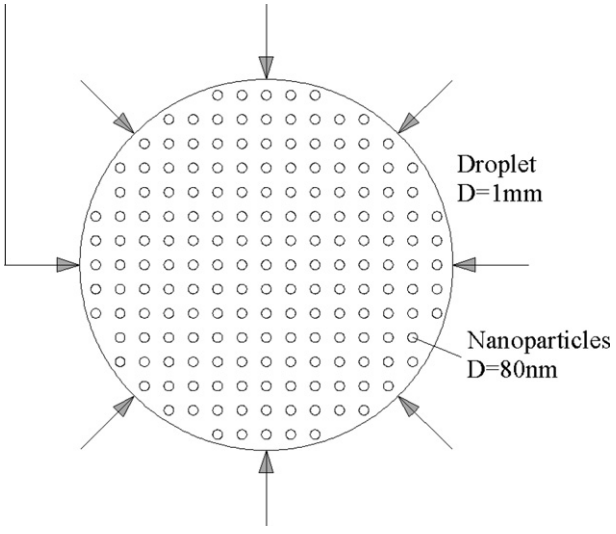

Fig. 12. Particle aggregation model in a vaporizing droplet.

According to Smoluchowski's classical work [20], the PBE, which describes the birth and death of aggregate as a result of collision and breakup, can be written as

$$\frac{dn_i}{dt} = \frac{1}{2}\sum_{j=1}^{i-1} \alpha_{j,i-j}\beta_{j,i-j} n_j n_{i-j} - \sum_{j=1}^{n} \alpha_{ij}\beta_{ij} n_i n_j - S_i n_i + \sum_{j=1}^{n} \Gamma_{ij} S_j n_j \qquad (1)$$

The left side of the equation expresses the variation rate of the number of i-fold aggregates, where n_i is the number of the i-fold aggregate and t is time. Note that the i-fold aggregate means a cluster that contains i original particles. The mass of the cluster is i times the mass of the original single particle. In the beginning, particles of the same size are uniformly distributed within the droplet. Throughout the evaporation process, aggregates of various sizes will be formed. For the aggregation of solid particles, no coalescence can occur, and thus the resulting clusters may have different structures [19]. It is extremely difficult to provide a detailed description of the aggregate structure, especially when hundreds or thousands of particles are involved. Thus we defined the size of the i-fold aggregates using a simplified way, as follows:

$$\frac{4}{3}\pi r_i^3 = i\frac{4}{3}\pi r_1^3 \qquad (2)$$

where r_1 is the initial particle radius and r_i is the nominal radius of the i-fold aggregates.

The first term on the right of the equation represents the rate of formation of the i-fold aggregates as a result of collision between any pair of aggregates, i–j and j. The collision efficiency and collision frequency between i and j folds are α_{ij} and β_{ij}. Summation in this way actually counts each collision twice, thus a factor of 0.5 is applied. The second term on the right of the equation accounts for loss of the i-fold aggregates as a result of collision and aggregation with other aggregates. The third term describes the breakup of the i-fold, where S_i represents the breakup rate. The fourth term stands for the contribution to i-fold from the breakup of any other folds, where Γ_{ij} is the distribution function of aggregate fragments.

Several assumptions were made in the model. First, only two-body collisions were considered following Smoluchowski's classic work [20]. This is a reasonable assumption because for dilute suspensions, the collisions by three or more bodies have a much lower frequency than the two-body collisions, and thus they can be neglected. Also, the particle aggregation process was simulated only for the first 50% of the droplet steady-state evaporation process. At a later stage, the particle concentration can be much higher because the droplet volume is decreased; thus the two-body collision assumption may not be valid under these conditions.

Second, we have shown in a previous study [8] that for nanosuspensions, the Brownian motion is mainly responsible for particle collision and aggregation. The rates of particle collision as a result of fluid transport (such as droplet surface regression and internal circulation) and differential settling are much smaller. However, for suspensions with micron-sized or larger particles, the fluid transport is more important than the Brownian motion. Because nanosized particles are of interest and were used in the experiments, only aggregation kernels resulting from the Brownian motion were considered in the model. Fluid motion can give a significant increase in the rate of particle intercollision where the colloids were subject to shear, e.g., by vigorous stirring or by turbulence [19]. In the present paper, however, droplets were under natural or very weak convection. The internal circulation caused by relative velocity between the gas and liquid phases is weak compared to that under high Reynolds number convections [21]. Thus fluid motion inside the droplet is less likely to make a significant contribution to particle collisions. It is important to note

that when the size of the aggregates is sufficiently large, the orthokinetic aggregation because of fluid transport can become dominant over perikinetic collisions.

Lastly, we assume that particle aggregation be a one-way process without breakup. This means that the last two terms on the right side of PDE are zero. This is a reasonable assumption because the breakup of aggregates is mainly brought about by hydrodynamic stresses [22], which is the fluid shear induced by fluid motion. The droplets in this study were vaporized under natural or very weak convection. Thus fluid shear induced by internal motion is weak, especially compared to that under high Reynolds number convection. In all, the breakup of particle aggregates is less likely to make a significant contribution to particle collisions.

The collision frequency β_{ij} between the i and j folds can be expressed as [20]

$$\beta_{ij} = \frac{2kT}{3\mu}\frac{(r_i + r_j)^2}{r_i r_j} \tag{3}$$

where k is the Boltzmann constant, T is the temperature, μ is the viscosity of the liquid, and r_i and r_j are the radii of particles i and j, respectively. The collision efficiency α_{ij} is assumed to be unity, which means that every collision results in an attachment of particles. In reality, collision efficiency can be significantly reduced because of repulsive forces from colloidal interaction, e.g., the steric interaction as a result of adding a surfactant. Another main factor is the hydrodynamic effect. As particles become very close to one another, it becomes increasingly difficult for the base liquid between them to drain out. This will hinder the approach of the particles and thus reduce collision efficiency. Overall, collision efficiency mainly depends on the forces between the particles and the hydrodynamic effect. It is extremely difficult to provide an accurate expression of collision efficiency [19]. In a recent study by Chen and You [23], different forces between the particles were considered to determine it, including van der Waals force, elastic deformation force, and electrostatic force. The results show that the collision efficiency increases when the particle size decreases. When the size of the particle is less than 100 nm, the collision efficiency is approaching unity. Here we used unity for the collision efficiency as an ideal situation. This means that the real aggregation process could be much slower than the ideal process we are simulating here.

Based on these assumptions, the discrete form of the population balance equations for every i-fold was numerically solved to get the temporal evolution of the aggregates with various size. The ordinary differential equations were solved numerically using third-order Runge–Kutta methods. The initial values (for example, with 0.5 wt.% nano-Al uniformly distributed within a droplet with an initial diameter of 1 mm) were set as $n_1 = 3 \times 10^9$, $n_2 = n_3 = \cdots = n_{3\times10^9} = 0$ at $t = 0$, where n_i means the number of i-fold in the droplet. It is noted that droplet size regression was also considered in the aggregation model, and this will be discussed further in the next section.

3.6.2. Modeling results

We first discuss the aggregation process inside an ethanol-based droplet. Fig. 13 shows the time history of the aggregate number for 7 representative aggregates ranging from 1-fold to 10,000-fold. The initial condition is the same as that in Fig. 6 (line with square dot) – an ethanol-based droplet with 0.5 wt.% nano-Al addition under natural evaporation at 300 K. Under such circumstances, 3 billion particles were suspended inside the droplet initially at $t = 0$ s. The term "i-fold" means the aggregates containing i particles.

The 1-fold particles (primary particles) disappear quickly by forming two- or more-particle clusters, as indicated by an earlier steep drop of the 1-fold curve ($t < 5$ s). The decrease rate of the 1-fold number slows at later times ($t > 20$ s). By the end of the computation time, which is about 60 s, only 147 individual particles are left. All other folds have the same trend: the number of the i-fold increases first, reaches a maximum value at a critical time, and then decreases gradually. The critical time occurs later for the higher fold than it does for the lower fold. For example, the critical time corresponding to the maximum number occurs at $t = 1.8$ s for 100-fold, at $t = 8.95$ s for 1000-fold, and at $t = 83$ s for 8000-fold. As time goes on, the population of smaller clusters decreases and that of larger clusters increases as a result of collisions between clusters. Another observation is that the number of all folds tends to reach an equilibrium point around 100 s, shown as a "band shape" in Fig. 13.

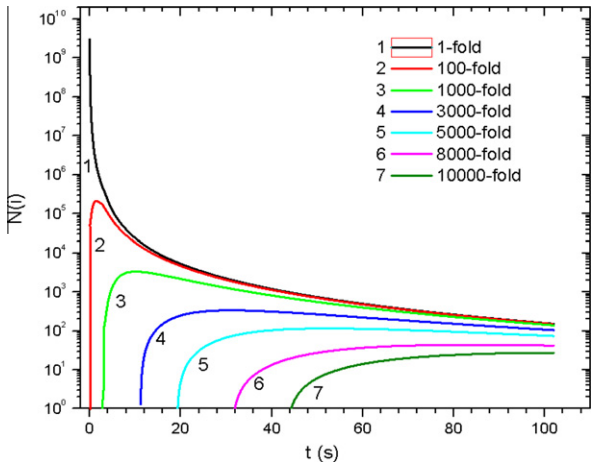

Fig. 13. Time history of number for i-fold aggregates inside an ethanol-based droplet with 0.5 wt.% nano-Al addition under natural convection of 300 K. At $t = 0$ s, the droplet has a diameter of 1 mm, the particle size is 80 nm, and there are 3 billion particles present within the droplet.

The particle aggregation process inside an evaporating droplet under natural convection is seen to be a continuous and slow process. Larger aggregates were produced, and smaller aggregates disappeared because of collisions among them. The structures of large aggregates can be complicated, resulting from the random combination of individual particles that may interlink with one another to form even more-complicated structures. The existence of large aggregate structures tends to inhibit internal diffusion of the liquid fuel from inside toward the droplet surface. Consequently, the droplet evaporation rate is reduced. The reduction in evaporation rate is more significant when larger aggregates are formed. This explains the D^2-law deviation phenomenon observed in the experiment.

Next, we discuss the effect of particle concentration on droplet evaporation. Fig. 14 shows the aggregate number as a function of time for 7 representative aggregates ranging from 1-fold to 10,000-fold for an ethanol-based droplet with 2.5 wt.% nano-Al addition under natural evaporation at 300 K. Fig. 14 shares some similarities with Fig. 13 (with 0.5% addition). However, there are differences. First, the time needed for the i-fold aggregate to form is shorter at higher particle concentrations than at lower ones. For example, the 5000-fold aggregates start to form at $t = 4.21$ s for the 2.5 wt.% nano-Al addition case, and at $t = 18.05$ s for the 0.5 wt.% nano-Al addition case. Moreover, the critical time corresponding to the maximum number of each fold appears earlier if the concentration of particles is higher. When the particle concentration is higher, the collision frequency between particles is also higher. As a result, large aggregate structures will form at earlier times and have a higher number density. This means that the suppression of droplet evaporation because of these large structures will occur earlier and will be more serious. And this explains the experimental observation that the evaporation curve under natural evaporation in Fig. 8 shows a more-obvious departure from the D^2-law compared to that in Fig. 6.

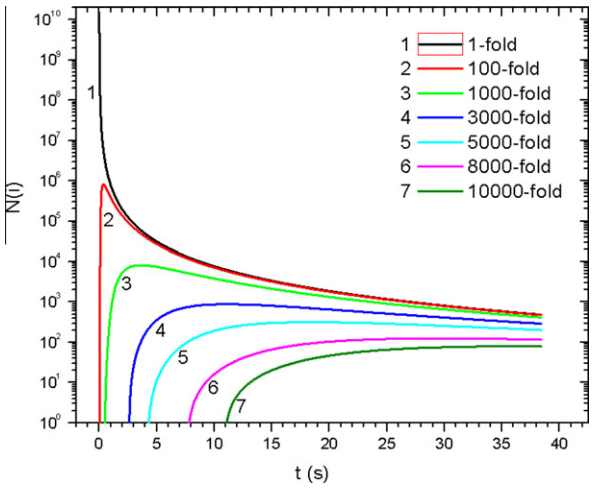

Fig. 14. Time history of number for *i*-fold aggregates inside an ethanol-based droplet with 2.5 wt.% nano-Al addition under natural convection of 300 K. At $t = 0$ s, the droplet has a diameter of 1 mm, the particle size is 80 nm, and there are 15 billion particles present within the droplet.

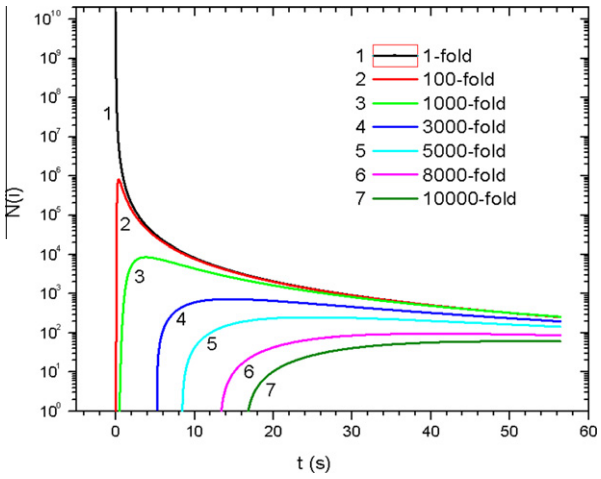

Fig. 16. Time history of number for *i*-fold aggregates inside an n-decane-based droplet with 2.5 wt.% nano-Al addition under weak forced convection of 300 K. At $t = 0$ s, the droplet has a diameter of 1 mm, the particle size is 80 nm, and there are 3 billion particles present within the droplet.

Next we will discuss the effect of the base fuel on droplet evaporation. Fig. 15 shows the temporal evolution of the aggregate number for 7 representative aggregates ranging from 1-fold to 10,000-fold for an n-decane-based droplet with 0.5 wt.% nano-Al addition under weak convection at 300 K. Note that this corresponds to the experimental result shown in Fig. 9 (line with square dot). Fig. 16 shows the computational results for an n-decane-based droplet with 2.5 wt.% nano-Al, which corresponds to the experimental results shown in Fig. 10 (line with square dot). Similar results can be concluded for the n-decane-based droplets in Figs. 15 and 16. For instance, at higher particle concentrations the departure from D^2-law is more obvious and the reduction of the evaporation rate is bigger. Comparing to the results in Fig. 13, we can see that large aggregates take a longer time to form for n-decane-based droplets than for ethanol-based droplets. For example, the time needed to form the 10,000-fold aggregates is 72.18 s for an n-decane-based droplet, which is 42.10 s for an ethanol-based droplet. Note the lifetime of the n-decane-based droplet (about 650 s) is longer than that of the ethanol-based droplet (about 350 s).

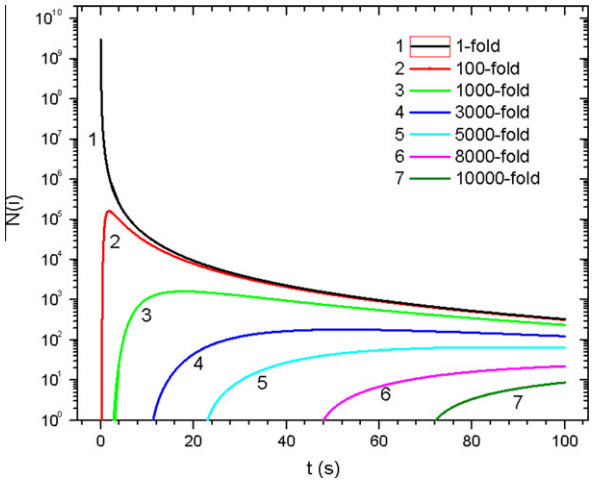

Fig. 15. Time history of number for *i*-fold aggregates inside an n-decane-based droplet with 0.5 wt.% nano-Al addition under weak forced convection of 300 K. At $t = 0$ s, the droplet has a diameter of 1 mm, the particle size is 80 nm, and there are 3 billion particles present within the droplet.

In summary, the modeling results show that the particle aggregation process inside an evaporation droplet is a continuous and slow process under natural convection or weak forced convection. During earlier times, smaller-sized aggregates that consist of only a few particles dominate the population. Later, larger-sized aggregates start to form, and they may eventually dominate the population. The present experiment deals with the evaporation of nanofluid-type fuels at natural and weak convections. The characteristic time required to form large aggregates is much longer than under strong convection, e.g., combustion. Previous studies on droplet combustion of nanofluid fuels have shown that a shell was formed during the combustion process as a result of particle aggregation, and the existence of the shell inhibited the diffusion process of the base fuel and thus reduced the burning rate [8]. We can expect that droplet evaporation will be affected when large aggregate structures are present within the droplet. The large aggregates inhibit diffusion and thus decrease the evaporation rate. If the droplet lifetime is longer than or at least comparable to the characteristic aggregation time, the particle aggregation process will have an effect on the evaporation. Moreover, the continuous change in droplet evaporation rate would be expected as a result of the continuous aggregation process: the number of larger aggregate structures increases with time; the number of smaller aggregates decreases. If the droplet lifetime is shorter than the characteristic aggregation time, it means that during the droplet evaporation process, smaller-sized aggregates dominate the population, and larger ones have not yet had sufficient time to form. Under these circumstances, particle aggregation would have the least impact on droplet evaporation because the aggregate structure that consists of only a few particles would have the least impact on diffusion. This explains why under certain conditions (such as strong forced convection at higher temperatures, or with the use of lower-boiling-point fuels as the base fluid), deviation from the D^2-law was not observed because the droplet evaporates faster than the particle aggregate in such conditions.

4. Conclusions

The effect of added aluminum nanoparticles on the evaporation characteristics of fuel droplets were investigated under both natural and forced convections. The droplet evaporation rate was measured by considering various base fuels, at varying particle concentrations and at convective flow temperatures. Furthermore,

the particle aggregation process was numerically modeled to understand the potential role of particle aggregation on droplet evaporation rate. The evolution history of particle aggregates (including aggregation size and distribution) was obtained by solving the PBEs, which accounts for various events taking place between particles in the population, e.g., aggregation and breakage. The major conclusions are as follows.

As expected, the evaporation of pure liquid droplets such as ethanol and n-decane follows the classical D^2-law under all test conditions. For ethanol-based nanofluids under weak convection at three flow temperatures (300 K, 330 K, and 380 K), the evaporation also follows the D^2-law. A departure from it was observed under natural convection at 300 K. The droplet evaporation rate was gradually slowed. The reduction in the evaporation rate is 30% for 0.5 wt.% particle addition and 50% for 2.5 wt.% particle addition.

For n-decane-based nanofluids, the D^2-law holds when droplets are vaporized under weak convection at higher temperatures (e.g., 380 K). A departure from the D^2-law was observed under both natural convection at 300 K and weak forced convection at 300 K for n-decane droplets with 0.5 wt.% nano-Al. For n-decane droplets with 2.5 wt.% nano-Al, a departure was observed under weak convection at 300 K and 320 K. These results show that the D^2-law deviation phenomenon is more prevalent at higher particle concentrations and for base fluids that have higher boiling points. A common feature among the conditions for which the deviation was observed is the long droplet lifetime.

The modeling results suggest that the D^2-law deviation phenomena and the continuous decrease in droplet evaporation rate could be a result of particle aggregation inside a vaporizing droplet, which is a rather slow process under natural or weak convection. If the droplet lifetime is longer or comparable to the characteristic aggregation time, large aggregates are formed during the droplet evaporation process, which could inhibit diffusion and thus reduce the evaporation rate. On the contrary, if the droplet lifetime is shorter than the characteristic aggregation time, smaller-sized aggregates dominate the population, and they have the least impact on diffusion and evaporation. In such circumstances, larger aggregates that suppress droplet evaporation have not yet had sufficient time to form; deviation from the D^2-law was therefore not observed in these circumstances.

Acknowledgment

This work has been supported by the Army Research Office (ARO) with Dr. Ralph Anthenien as the technical monitor.

References

[1] S.U.S. Choi, Nanofluids: from vision to reality through research, J. Heat Transfer – Trans. ASME 131 (3) (2009) 033106. 1–9.
[2] X.W. Wang, X.F. Xu, S.U.S. Choi, Thermal conductivity of nanoparticle-fluid mixture, J. Thermophys. Heat Transfer 13 (4) (1999) 474–480.
[3] W.H. Yu, D.M. France, J.L. Routbort, S.U.S. Choi, Review and comparison of nanofluid thermal conductivity and heat transfer enhancements, Heat Transfer Eng. 29 (5) (2008) 432–460.
[4] S. Senthilraja, M. Karthikeyan, R. Gangadevi, Nanofluid applications in future automobiles: comprehensive review of existing data, Nano-Micro Lett. 2 (4) (2010) 306–310.
[5] R.A. Yetter, G.A. Risha, S.F. Son, Metal particle combustion and nanotechnology, Proc. Combust. Inst. 32 (2009) 1819–1838.
[6] D. Jackson, D. Davidson, R. Hanson, Application of an aerosol shock tube for the kinetic studies of n-dodecane/nano-aluminum slurries, in: 44th AIAA/ASME/SAE/ASEE Joint Propulsion Conference and Exhibit, Hartford, CT, United States, 2008.
[7] H. Tyagi, P.E. Phelan, R. Prasher, R. Peck, T. Lee, J.R. Pacheco, P. Arentzen, Increased hot-plate ignition probability for nanoparticle-laden diesel fuel, Nano Lett. 8 (5) (2008) 1410–1416.
[8] Y. Gan, L. Qiao, Combustion characteristics of fuel droplets with addition of nano and micron-sized aluminum particles, Combust. Flame 158 (2) (2011) 354–368.
[9] S.R. Turns, An Introduction to Combustion: Concepts and Application, McGraw-Hill Science, 2006.
[10] C.H. Chon, S. Paik, J.B. Tipton, K.D. Kihm, Effect of nanoparticle sizes and number densities on the evaporation and dryout characteristics for strongly pinned nanofluid droplets, Langmuir 23 (6) (2007) 2953–2960.
[11] K. Sefiane, R. Bennacer, Nanofluids droplets evaporation kinetics and wetting dynamics on rough heated substrates, Adv. Colloid Interface Sci. 147–48 (2009) 263–271.
[12] R.H. Chen, T.X. Phuoc, D. Martello, Effects of nanoparticles on nanofluid droplet evaporation, Int. J. Heat Mass Transfer 53 (19-20) (2010) 3677–3682.
[13] A. Gedanken, Using sonochemistry for the fabrication of nanomaterials, Ultrason. Sonochem. 11 (2) (2004) 47–55.
[14] D.H. Napper, Steric stabilization, J. Colloid Interf. Sci. 58 (2) (1977) 390–407.
[15] Y.J. Shin, Y.H. Shen, Preparation of coal slurry with organic solvents, Chemosphere 68 (2) (2007) 389–393.
[16] I. Langmuir, The evaporation of small spheres, Phys. Rev. 12 (5) (1918) 368–370.
[17] P. Taboada-Serrano, C.J. Chin, S. Yiacoumi, C. Tsouris, Modeling aggregation of colloidal particles, Curr. Opin. Colloid Interface Sci. 10 (3–4) (2005) 123–132.
[18] S. Kumar, D. Ramkrishna, On the solution of population balance equations by discretization – I. A fixed pivot technique, Chem. Eng. Sci. 51 (8) (1996) 1311–1332.
[19] J.H. Fendler, I. Dekany, Nanoparticles in Solids and Solutions, Kluwer Academic Publishers, Boston, 1996.
[20] M. Smoluchowski, Mathematical theory of the kinetics of the coagulation of colloidal solutions, Z. Phys. Chem. 92 (1917) 129–168.
[21] C.K. Law, Recent advances in droplet vaporization and combustion, Prog. Energy Combust. Sci. 8 (3) (1982) 171–201.
[22] J.J. Zhang, X.Y. Li, Modeling particle-size distribution dynamics in a flocculation system, AIChE J. 49 (7) (2003) 1870–1882.
[23] Z.L. Chen, Z.J. You, New expression for collision efficiency of spherical nanoparticles in Brownian coagulation, Appl. Math. Mech. – English Ed. 31 (7) (2010) 851–860.